MAE 557 Mini-Project Two

Yu Shuai

October 23, 2025

1 Governing equations for the 2D compressible lid-driven cavity flow

Generally speaking, the governing equations of a single-component compressible flow consist of:

- the continuity equation
- the momentum equation
- the energy equation
- the equation of state

Here, since the flow is viscous, the kinetic energy is inherently not conservative. Consequently, the momentum equationis not secondary conservative. To avoid introducing spurious temperature fluctuations, here we choose the energy equation to be the equation of internal energy.

The mathematical form of governing equations are then given as follows:

$$\frac{\partial}{\partial t}\rho + \frac{\partial}{\partial x_j}(\rho u_j) = 0, \tag{1a}$$

$$\frac{\partial}{\partial t}(\rho u_i) + \frac{\partial}{\partial x_j}(\rho u_j u_i) = \frac{\partial}{\partial x_j}\left(-p\delta_{ij} + \mu\left(\frac{\partial u_i}{\partial x_j} + \frac{\partial u_j}{\partial x_i} - \frac{2}{3}\frac{\partial u_k}{\partial x_k}\delta_{ij}\right)\right), \tag{1b}$$

$$\frac{\partial}{\partial t}(\rho e) + \frac{\partial}{\partial x_j}(\rho u_j e) = \frac{\partial}{\partial x_j}\left(\lambda\frac{\partial T}{\partial x_j}\right) - p\frac{\partial u_k}{\partial x_k} + 2\mu\left(\frac{1}{2}\left(\frac{\partial u_i}{\partial x_j} + \frac{\partial u_j}{\partial x_i}\right) - \frac{1}{3}\frac{\partial u_k}{\partial x_k}\delta_{ij}\right)^2, \tag{1c}$$

$$p = \rho R T \tag{1d}$$

$$e = \frac{1}{\gamma - 1} RT, \tag{1e}$$

where $x_1, x_2 \in [0, L]$ are horizontal and vertical spatial coordinates respectively, ρ is the density, $u_i (i = 1, 2)$ are velocity components, p is the pressure, and e is the internal energy. $\mu = \rho\nu$ is the dynamical viscosity, λ is the thermal diffusivity, $R = 287\,\mathrm{J/(kg \cdot K)}$ is the specific gas constant, $\gamma = c_p/c_v$ is the ratio of specific heats.

Initially, the flow is stationary, i.e., $u(x_1, x_2, t = 0) = 0$ for all x_1, x_2. So, we can assume that the density is initially uniform $\rho(x_1, x_2, t = 0) = \rho_0$ for all x_1, x_2. The initial pressure and temperature are uniformly given $p(x_1, x_2, t = 0) = p_0 = 1\mathrm{bar} = 10^5\,\mathrm{Pa}$ and $T(x_1, x_2, t = 0) = T_0 = 300\,\mathrm{K}$. From these values, we can utilize the equation of state (1d) to obtain $\rho_0 = 100000/86100 \approx 1.161\,(\mathrm{kg/m^3})$

For the boundary conditions, the horizontal velocity on the top wall satisfy $u_1(x_1, x_2 = L, t) = u_w(t) = U_w \sin(\omega t)$, while the velocities on all other walls are 0 satisfying the no-slip and no-penetration boundary conditions. Since the walls are isothermal, we have $T(x_1 = 0, x_2, t) = T(x_1, x_2 = 0, t) = T(x_1 = L, x_2, t) = T(x_1, x_2 = L, t) = 300\,\mathrm{K}$. The boundary conditions of density are given following the Navier-Stokes characteristic boundary conditions (NSCBC, see eq. (24)-(28) in [1]). Since the walls are no-slip no-penetration solid walls, we have two fluxes equal to each other following the so-called local one-dimensional inviscid relations

$$(u_n - a)\left(\frac{\partial p}{\partial n} - \rho a\frac{\partial u_n}{\partial n}\right) = (u_n + a)\left(\frac{\partial p}{\partial n} + \rho a\frac{\partial u_n}{\partial n}\right). \tag{2}$$

Here, n is the normal direction to the boundary pointing outwards from the computational domain, and a is the speed of sound. Substituting $u_n = 0$ into (2), we find that the normal gradient of pressure is 0

$$\frac{\partial p}{\partial n} = 0.$$

Since $p = \rho RT$, we now have

$$\rho\frac{\partial T}{\partial n} + T\frac{\partial \rho}{\partial n} = 0 \tag{3}$$

at the boundaries, from which we can compute the density at the wall using the information from interior points.

Next, we non-dimensionalize our governing equations. Let $\rho^* = \rho/\rho_0$, $x_j^* = x_j/L$ and $u_j^* = u_j/U_w$, we have $t^* = t/t_c = U_w t/L$ and $t_c = L/U_w$, where all quantities with the superscript $*$ are dimensionless. The continuity equation (1a) then becomes

$$\frac{\partial \rho^*}{\partial t^*} + \frac{\partial}{\partial x_j^*}(\rho^* u_j^*) = 0. \tag{4}$$

Additionally, if we let $p^* = p/p_c$ where $p_c = \rho_0 U_w^2$, then the momentum equation (1b) becomes

$$\frac{\partial}{\partial t^*}(\rho^* u_i^*) + \frac{\partial}{\partial x_j^*}(\rho^* u_j^* u_i^*) = -\frac{\partial p^*}{\partial x_i^*} + \frac{1}{\mathrm{Re}}\frac{\partial}{\partial x_j^*}\left(\rho^*\left(\frac{\partial u_i^*}{\partial x_j^*} + \frac{\partial u_j^*}{\partial x_i^*} - \frac{2}{3}\frac{\partial u_k^*}{\partial x_k^*}\delta_{ij}\right)\right), \tag{5}$$

where $\mathrm{Re} = U_w L/\nu$ is the Reynolds number with ν the constant kinematic viscosity. Additionally, if we let $e^* = e/e_c$ where $e_c = RT_c/(\gamma - 1)$ and $T_c = T_0 = 300\,\mathrm{K}$, and let the reference speed of sound $a_c = \sqrt{\gamma R T_c}$, then the internal energy equation (1c) becomes:

$$\frac{\partial}{\partial t^*}(\rho^* e^*) + \frac{\partial}{\partial x_j^*}(\rho^* u_j^* e^*) = \frac{\gamma}{\mathrm{PrRe}}\frac{\partial}{\partial x_j^*}\left(\rho^*\frac{\partial T^*}{\partial x_j^*}\right) - \gamma(\gamma-1)\mathrm{Ma}^2 p^*\frac{\partial u_k^*}{\partial x_k^*} + \frac{2\mathrm{Ma}^2\gamma(\gamma-1)}{\mathrm{Re}}\rho^*\left(\frac{1}{2}\left(\frac{\partial u_i^*}{\partial x_j^*} + \frac{\partial u_j^*}{\partial x_i^*}\right) - \frac{1}{3}\frac{\partial u_k^*}{\partial x_k^*}\delta_{ij}\right)^2, \tag{6}$$

where $\mathrm{Pr} = \rho c_p \nu/\lambda$ is the constant Prandtl number with c_p the constant-pressure specific heat and λ the thermal conductivity, γ the ratio of specific heats, $\mathrm{Ma} = U_w/a_c$ the Mach number with $a_c = \sqrt{\gamma R T_c}$.

Apart from non-dimensionalizing the equations, we also need to non-dimensionalize the boundary conditions and initial conditions. For the boundary conditions, we know that the horizontal velocity on the top wall is given by $u_1(x_1, L, t) = U_w \sin(\omega t)$, so we have $u_1^*(x_1^*, 1, t^*) = \sin((\omega L/U_w)t^*) = \sin(2t^*/Re)$. Similarly, the boundary conditions for the dimensionless temperature is $T^*(0, x_2^*, t^*) = T^*(x_1^*, 0, t^*) = T^*(1, x_2^*, t^*) = T^*(x_1^*, 1, t^*) = 1$. For the initial conditions, we have $p^*(x_1^*, x_2^*, 0) = p_0/(\rho_0 U_w^2) = 1/(\gamma \mathrm{Ma}^2)$.

Finally, we combine the dimensionless governing equations, initial conditions, physical boundary conditions and characteristic boundary conditions to form the following problem:

$$\frac{\partial \rho^*}{\partial t^*} + \frac{\partial}{\partial x_j^*}(\rho^* u_j^*) = 0, \tag{7a}$$

$$\frac{\partial}{\partial t^*}(\rho^* u_i^*) + \frac{\partial}{\partial x_j^*}(\rho^* u_j^* u_i^*) = -\frac{\partial p^*}{\partial x_i^*} + \frac{1}{\mathrm{Re}}\frac{\partial}{\partial x_j^*}\left(\rho^*\left(\frac{\partial u_i^*}{\partial x_j^*} + \frac{\partial u_j^*}{\partial x_i^*} - \frac{2}{3}\frac{\partial u_k^*}{\partial x_k^*}\delta_{ij}\right)\right), \tag{7b}$$

$$\frac{\partial}{\partial t^*}(\rho^* e^*) + \frac{\partial}{\partial x_j^*}(\rho^* u_j^* e^*) = \frac{\gamma}{\mathrm{PrRe}}\frac{\partial}{\partial x_j^*}\left(\rho^*\frac{\partial T^*}{\partial x_j^*}\right) - \gamma(\gamma-1)\mathrm{Ma}^2 p^*\frac{\partial u_k^*}{\partial x_k^*} + \frac{2\mathrm{Ma}^2\gamma(\gamma-1)}{\mathrm{Re}}\rho^*\left(\frac{1}{2}\left(\frac{\partial u_i^*}{\partial x_j^*} + \frac{\partial u_j^*}{\partial x_i^*}\right) - \frac{1}{3}\frac{\partial u_k^*}{\partial x_k^*}\delta_{ij}\right)^2, \tag{7c}$$

$$p^* = \frac{1}{\gamma \mathrm{Ma}^2}\rho^* T^*, \tag{7d}$$

$$e^* = T^*, \tag{7e}$$

$$u_1^*(x_1^*, 1, t^*) = \sin(2t^*/\mathrm{Re}), u_1^*(0, x_2^*, t^*) = u_1^*(x_1^*, 0, t^*) = u_1^*(1, x_2^*, t^*) = 0, \tag{7f}$$

$$u_2^*(x_1^*, 1, t^*) = u_2^*(0, x_2^*, t^*) = u_2^*(x_1^*, 0, t^*) = u_2^*(1, x_2^*, t^*) = 0, \tag{7g}$$

$$T^*(0, x_2^*, t^*) = T^*(x_1^*, 0, t^*) = T^*(1, x_2^*, t^*) = T^*(x_1^*, 1, t^*) = 1, \tag{7h}$$

$$\rho^*\frac{\partial T^*}{\partial n^*} + T^*\frac{\partial \rho^*}{\partial n^*} = 0 \quad \text{at walls}, \tag{7i}$$

$$\rho^*(x_1^*, x_2^*, 0) = 1, \tag{7j}$$

$$T^*(x_1^*, x_2^*, 0) = 1, \tag{7k}$$

$$u_1^*(x_1^*, x_2^*, 0) = u_2^*(x_1^*, x_2^*, 0) = 0, \tag{7l}$$

$$\mathrm{Re} = 100, \quad \gamma = 1.4, \quad \mathrm{Ma} = 0.025, \quad \mathrm{Pr} = 0.7. \tag{7m}$$

Or, one can rewrite the equations in a componentwise form:

$$\frac{\partial \rho^*}{\partial t^*} + \frac{\partial}{\partial x_1^*}(\rho^* u_1^*) + \frac{\partial}{\partial x_2^*}(\rho^* u_2^*) = 0, \tag{8a}$$

$$\frac{\partial}{\partial t^*}(\rho^* u_1^*) + \frac{\partial}{\partial x_1^*}(\rho^* u_1^* u_1^*) + \frac{\partial}{\partial x_2^*}(\rho^* u_2^* u_1^*) = -\frac{\partial p^*}{\partial x_1^*} + \frac{1}{\mathrm{Re}}\frac{\partial}{\partial x_1^*}\left(\rho^*\left(\frac{\partial u_1^*}{\partial x_1^*} + \frac{\partial u_1^*}{\partial x_1^*} - \frac{2}{3}(\frac{\partial u_1^*}{\partial x_1^*} + \frac{\partial u_2^*}{\partial x_2^*})\right)\right)$$
$$+ \frac{1}{\mathrm{Re}}\frac{\partial}{\partial x_2^*}\left(\rho^*\left(\frac{\partial u_1^*}{\partial x_2^*} + \frac{\partial u_2^*}{\partial x_1^*}\right)\right), \tag{8b}$$

$$\frac{\partial}{\partial t^*}(\rho^* u_2^*) + \frac{\partial}{\partial x_1^*}(\rho^* u_1^* u_2^*) + \frac{\partial}{\partial x_2^*}(\rho^* u_2^* u_2^*) = -\frac{\partial p^*}{\partial x_2^*} + \frac{1}{\mathrm{Re}}\frac{\partial}{\partial x_1^*}\left(\rho^*\left(\frac{\partial u_2^*}{\partial x_1^*} + \frac{\partial u_1^*}{\partial x_2^*}\right)\right)$$
$$+ \frac{1}{\mathrm{Re}}\frac{\partial}{\partial x_2^*}\left(\rho^*\left(\frac{\partial u_2^*}{\partial x_2^*} + \frac{\partial u_2^*}{\partial x_2^*} - \frac{2}{3}(\frac{\partial u_1^*}{\partial x_1^*} + \frac{\partial u_2^*}{\partial x_2^*})\right)\right), \tag{8c}$$

$$\frac{\partial}{\partial t^*}(\rho^* e^*) + \frac{\partial}{\partial x_1^*}(\rho^* u_1^* e^*) + \frac{\partial}{\partial x_2^*}(\rho^* u_2^* e^*) = \frac{\gamma}{\mathrm{PrRe}}\frac{\partial}{\partial x_1^*}\left(\rho^*\frac{\partial T^*}{\partial x_1^*}\right) + \frac{\gamma}{\mathrm{PrRe}}\frac{\partial}{\partial x_2^*}\left(\rho^*\frac{\partial T^*}{\partial x_2^*}\right) - \gamma(\gamma-1)\mathrm{Ma}^2 p^*\left(\frac{\partial u_1^*}{\partial x_1^*} + \frac{\partial u_2^*}{\partial x_2^*}\right)$$
$$+ \frac{2\mathrm{Ma}^2\gamma(\gamma-1)}{\mathrm{Re}}\rho^*\left(\left(\frac{\partial u_1^*}{\partial x_1^*}\right)^2 + \left(\frac{\partial u_2^*}{\partial x_2^*}\right)^2 + \frac{1}{2}\left(\frac{\partial u_1^*}{\partial x_2^*} + \frac{\partial u_2^*}{\partial x_1^*}\right)^2 - \frac{1}{3}\left(\frac{\partial u_1^*}{\partial x_1^*} + \frac{\partial u_2^*}{\partial x_2^*}\right)^2\right). \tag{8d}$$

2 Choose appropriate finite difference operators for the spatial operators

Since the problem is a low-Reynolds number flow, the dispersion error from spatial discretization schemes will rapidly fade away due to high dissipation. Therefore, the simplest approach is to adopt central schemes.

For the first-order spatial derivative, we choose the second-order central scheme such that for interior grid points $(i_1, i_2), i_1 \neq 0, i_1 \neq N_x, i_2 \neq 0, i_2 \neq N_y$, we have

$$\frac{\partial (\cdot)^j_{i_1,i_2}}{\partial x_1} \approx \frac{(\cdot)^j_{i_1+1,i_2} - (\cdot)^j_{i_1-1,i_2}}{2\Delta x_1}, \tag{9a}$$

$$\frac{\partial (\cdot)^j_{i_1,i_2}}{\partial x_2} \approx \frac{(\cdot)^j_{i_1,i_2+1} - (\cdot)^j_{i_1,i_2-1}}{2\Delta x_2}, \tag{9b}$$

where the coordinates of the grid point are $(x_1, x_2)_{i_1,i_2} = (i_1\Delta x_1, i_2\Delta x_2), i_1 = 0, 1, ..., N_{x_1}, i_2 = 0, 1, ..., N_{x_2}$. $\Delta x_1 = 1/N_{x_1}$ and $\Delta x_2 = 1/N_{x_2}$ are dimensionless spacing on two directions. It is worth mentioning that we formulate the central scheme for the second-order spatial derivative in the form of $\partial(\rho\partial u/\partial x)/\partial x$ as follows: First, we evaluate $\rho\partial u/\partial x$ at $(i_1 + 1/2, i_2)$ and $(i_1 - 1/2, i_2)$ via interpolation and central differencing, such that

$$\rho_{i_1+\frac{1}{2},i_2}\left(\frac{\partial u}{\partial x_1}\right)_{i_1+\frac{1}{2},i_2} \approx \frac{\rho_{i_1,i_2} + \rho_{i_1+1,i_2}}{2}\frac{u_{i_1+1,i_2} - u_{i_1,i_2}}{\Delta x_1}, \tag{10a}$$

$$\rho_{i_1-\frac{1}{2},i_2}\left(\frac{\partial u}{\partial x_1}\right)_{i_1-\frac{1}{2},i_2} \approx \frac{\rho_{i_1-1,i_2} + \rho_{i_1,i_2}}{2}\frac{u_{i_1,i_2} - u_{i_1-1,i_2}}{\Delta x_1}. \tag{10b}$$

Afterwards, we perform central differencing again to obtain the approximation

$$\begin{aligned}\left(\frac{\partial}{\partial x_1}\left(\rho\frac{\partial u}{\partial x_1}\right)\right)_{i_1,i_2} &\approx \frac{\rho_{i_1+\frac{1}{2},i_2}(\partial u/\partial x_1)_{i_1+\frac{1}{2},i_2} - \rho_{i_1-\frac{1}{2},i_2}(\partial u/\partial x_1)_{i_1-\frac{1}{2},i_2}}{\Delta x_1} \\ &\approx \frac{\rho_{i_1,i_2} + \rho_{i_1+1,i_2}}{2}\frac{u_{i_1+1,i_2} - u_{i_1,i_2}}{(\Delta x_1)^2} - \frac{\rho_{i_1-1,i_2} + \rho_{i_1,i_2}}{2}\frac{u_{i_1,i_2} - u_{i_1-1,i_2}}{(\Delta x_1)^2}.\end{aligned} \tag{11}$$

For the points on the domain boundaries, we only care about the values of density since the values of velocities and temperature are specified on the walls. To evaluate the normal derivatives in the density boundary conditions (7i), we adopt a one-sided second-order scheme to preserve global second-order accuracy while utilizing only points within the domain.

3 Choose appropriate temporal schemes and solution methods

In this work, we will choose the forward Euler method as the timestepper, since it is easy to implement in our code with a first-order temporal accuracy.

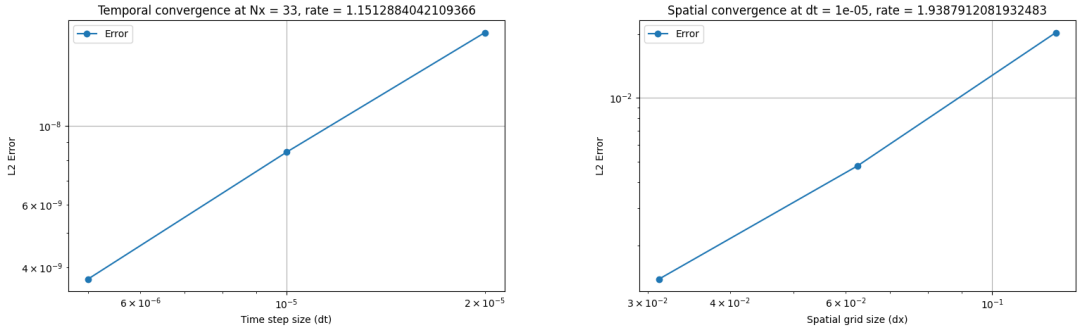

(a) (b)

Figure 1: Temporal and spatial rate of convergence for the FTCS solver of the cavity flow problem.

4 Expected approximate CFL limits

Since we are working on compressible flow problems, an upper limit of the CFL number for this 2D problem can be approximated by

$$C = \frac{(|u_1|_{\max} + a_{\max})\Delta t}{\Delta x_1} + \frac{(|u_2|_{\max} + a_{\max})\Delta t}{\Delta x_2}. \tag{12}$$

As we know, for a 1D linear advection PDE $\partial_t u + a\partial_x u = 0$ with the second-order central scheme for spatial derivatives and the forward Euler timestepper, the CFL number $a\Delta t/\Delta x$ has a limit of 1. So, we can utilize this conclusion to give the same form of upper bound for our CFL number:

$$\begin{aligned} C \leq 1 &\Longrightarrow \frac{(|u_1|_{\max} + a_{\max})\Delta t}{\Delta x_1} + \frac{(|u_2|_{\max} + a_{\max})\Delta t}{\Delta x_2} \leq 1, \\ &\Longrightarrow \frac{(|u_1^*|_{\max} + \mathrm{Ma}^{-1}\sqrt{T^*_{\max}})\Delta t^*}{\Delta x_1^*} + \frac{(|u_2^*|_{\max} + \mathrm{Ma}^{-1}\sqrt{T^*_{\max}})\Delta t^*}{\Delta x_2^*} \leq 1. \end{aligned} \tag{13}$$

In numerical implementations, we often want to restrict this upper bound by multiplying it with a relaxation parameter, such as 0.6.

5 Pseudo-code of the algorithm for lid-driven flow solver

See Algorithm 1 on the next page.

6 Analysis of convergence

We study the temporal convergence via fixing $N_x = N_y = 9$ (including both boundary points) and setting $\Delta t^* = 2\times10^{-5}, 10^{-5}, 5\times10^{-6}$. The error is evaluated as the root-mean-square of difference between the numerical solutions and a high-fidelity solution $\tilde{u}$ solved with $\Delta t^* = 10^{-6}$ on each grid point at the final time $t_f^* = 0.2$:

$$\epsilon = \frac{1}{N_{x_1}N_{x_2}} \sum_{i=0}^{N_{x_1}-1} \sum_{j=0}^{N_{x_2}-1} |\boldsymbol{u}^*(i\Delta x_1^*, j\Delta x_2^*, t_f^*) - \tilde{\boldsymbol{u}}^*(i\Delta x_1^*, j\Delta x_2^*, t_f^*)|_2^2, \tag{14}$$

where $\boldsymbol{u}^* = [\rho^*, u_1^*, u_2^*, T^*]$. Fig. 1(a) shows the rate of convergence for our forward-Euler temporal discretization, which is consistent with the temporal accuracy of the scheme.

Similarly, we study the spatial convergence via fixing $\Delta t^* = 10^{-5}$ and choose $N_x = N_y = 9, 17$ and 33, respectively. The error is then evaluated as the pointwise difference between the numerical solutions and a high-fidelity solution $\tilde{u}$ solved with $N_x = N_y = 65$ on the fixed location $(x_1^*, x_2^*) = (15/16, 15/16)$ at $t_f^* = 1.0$:

$$\epsilon = |\boldsymbol{u}^*(15/16, 15/16, t_f^*) - \tilde{\boldsymbol{u}}^*(15/16, 15/16, t_f^*)|_2^2. \tag{15}$$

Fig. 1(b) shows the rate of convergence for our central spatiall discretization, which is consistent with the second-order accuracy of the scheme.

Algorithm 1 FTCS Solver for 2D Compressible Lid-Driven Cavity Flow

Input: dimensionless constants Re, Ma, Pr, γ; number of grid points: N_{x_1}, N_{x_2} with grid spacing $\Delta x_1^* = 1/N_{x_1}$, $\Delta x_2^* = 1/N_{x_2}$; timestep Δt^* within the stability limit (13); number of timesteps N_t.
Initialize the grid-based variables: Set $\rho^*(i_1\Delta x_1^*, i_2\Delta x_2^*, 0) = 1$, $u_1^*(i_1\Delta x_1^*, i_2\Delta x_2^*, 0) = 0$, $u_2^*(i_1\Delta x_1^*, i_2\Delta x_2^*, 0) = 0$, and $T^*(i_1\Delta x_1^*, i_2\Delta x_2^*, 0) = 1$ for $i_1 = 0, 1, ..., N_{x_1}$, $i_2 = 0, 1, ..., N_{x_2}$ based on (7j)-(7m).
Define the conservative variables: Let $\mathbf{U} = (\rho^*, \rho^* u_1^*, \rho^* u_2^*, \rho^* e^*)$ be the variable to be advanced in time, where $e^* = T^*$.
Main timestepping loop:
for $j = 0$ to N_t **do** (**the forward Euler scheme**)
    $t^* \leftarrow j\Delta t^*$
    Evaluate the CFL number $C \leftarrow \frac{(|u_1^*|_{\max} + \mathrm{Ma}^{-1}\sqrt{T_{\max}^*})\Delta t^*}{\Delta x_1^*} + \frac{(|u_2^*|_{\max} + \mathrm{Ma}^{-1}\sqrt{T_{\max}^*})\Delta t^*}{\Delta x_2^*}$.
    if $C > 1$ **then**
        Warning: Timestep Δt^* violates the CFL stability limit.
        Exit.
    end if
    $\mathbf{U}(t^* + \Delta t^*) \leftarrow \mathbf{U}(t^*) + \Delta t^* \cdot \mathrm{RHS}(\mathbf{U}(t^*), t^*)$
    $\mathbf{U}(t^* + \Delta t^*) = \mathrm{ApplyBC}(\mathbf{U}(t^* + \Delta t^*), t^* + \Delta t^*)$
end for

---

function $\mathrm{RHS}(\mathbf{U}, t^*)$
    Initialization: Set $d\mathbf{U}/dt$ to be zero.
    Extract variables $\rho^*, u_1^*, u_2^*, T^*, e^*, p^*$ from the input $\mathbf{U}$.
    for $i_1 = 1$ to $N_{x_1} - 1$ **do**
        for $i_2 = 1$ to $N_{x_2} - 1$ **do**
            Calculate all first and second spatial derivatives on interior points using central schemes (9)-(11) to evaluate the RHS for continuity, momentum, and energy equations (8a)-(8d).
            Store results in the corresponding elements of $d\mathbf{U}/dt$.
        end for
    end for
    return $\frac{d\mathbf{U}}{dt}$.
end function

---

function ApplyBC$(\mathbf{U}, t^*)$
    Extract variables $\rho^*, u_1^*, u_2^*, T^*, e^*, p^*$ from the input $\mathbf{U}$.
    Apply the no-slip no-penetration boundary conditions for u_1^*, u_2^* on all walls according to (7f)(7g) using t^*.
    Apply the isothermal boundary conditions for T^* on all walls according to (7h).
    Update the density on the walls following the density boundary conditions (3).
    Re-assemble the matrix $\mathbf{U}$ based on updated variables.
    return $\mathbf{U}$.
end function

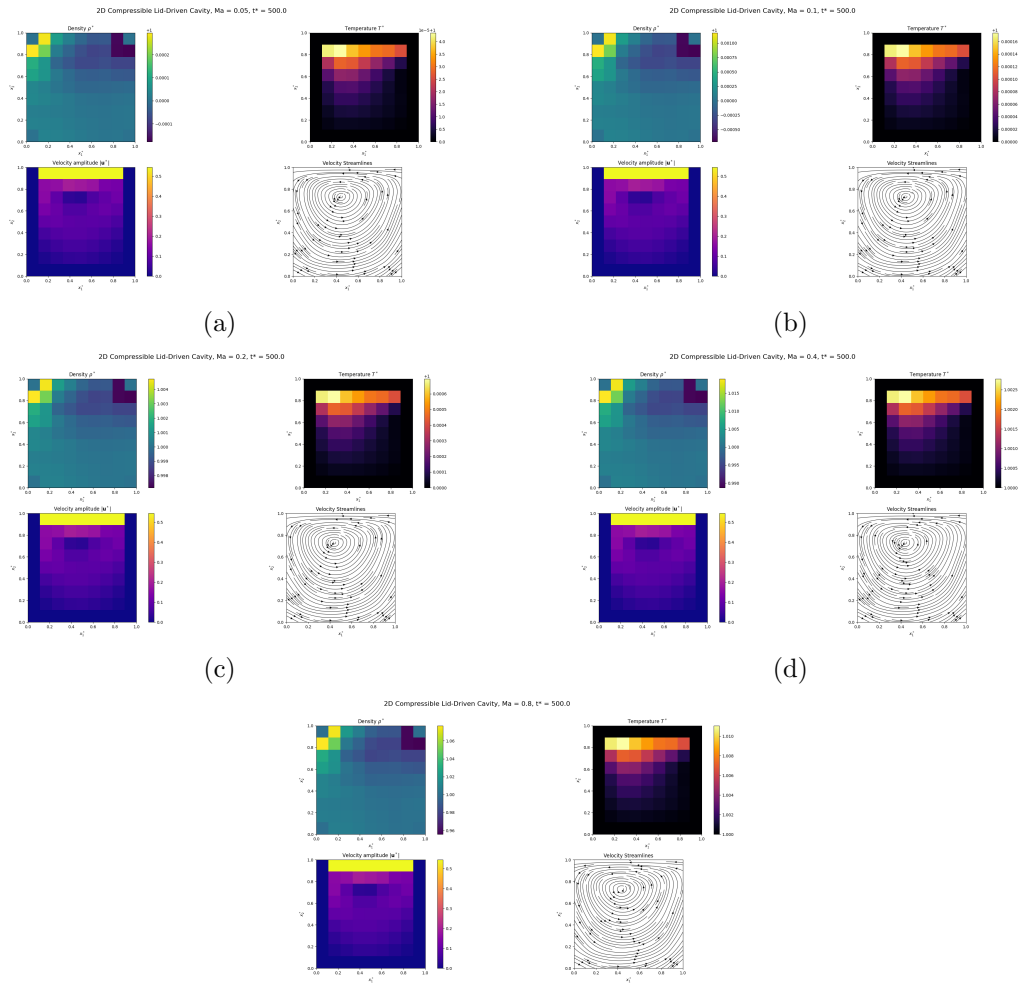

Figure 2: Solutions at $\omega t = 10$ (i.e. $2t^*/\mathrm{Re} = 10$) and $\mathrm{Ma} = 0.05, 0.1, 0.2, 0.4, 0.8$.

7 Qualitative changes of solutions and computational efficiency with increasing Mach number

Fig. 2 displays the solutions at $\omega t = (2/\mathrm{Re})t^* = 10$ with various Mach numbers $\mathrm{Ma} = 0.05, 0.1, 0.2, 0.4, 0.8$. From the figures, we find that as the Mach number increases, the variation of density and temperature gets intensified, which is consistent with the trend of increasing compressibility of the flow. Consequently, for the leftward-moving lid, the high-Mach-number flow field exhibits significant compressibility effects. An obvious density increase is observed at the top-left corner due to fluid compression, as the high-velocity flow entrained by the lid is stopped upon the stationary wall. Conversely, a density decrease occurs at the top-right corner, corresponding to flow expansion where the lid moves away. Furthermore, the high-speed compression at the top-left corner leads to a more intense heating. This local temperature rise is due to viscous dissipation within the high-shear region and thus the conversion of kinetic energy into internal energy via compressive work. Last but not least, we also observe that (not shown in the figure) the magnitude of the vertical velocity component near the top-left corner is smaller in high-Mach-number flows compared to the cases of low-Mach-number flows. This phenomenon is a direct consequence of compressibility. In the low-Mach-number case, the fluid acts rigidly such that the decrease of horizontal velocity while approaching the left wallmust be immediately converted into the vertical velocity component, resulting in strong downward acceleration. In the high-Mach-number case , however, the flow can now mitigate this violent redirection. As the fluid compresses, the local pressure builds up followed by a significant local increase in density. This change in pressure and density allows the fluid to "absorb" the incoming mass flux, thereby alleviating the kinematic necessity for a strong downward acceleration along the vertical wall.

For the computational efficiency, according to our CFL number limit (13), when the Mach number decreases, the timestep has to be decreased accordingly to keep the CFL number within the limit. Consequently, we need more timesteps to advance a low-Mach-number flow field for the same time compared to a high-Mach-number one, which takes more wall time to finish the computation. In our case where $N_{x_1} = N_{x_2} = 9$, the timestep for $\mathrm{Ma} = 0.05, 0.1, 0.2, 0.4, 0.8$ is $\Delta t^* = 5 \times 10^{-5}, 2.5 \times 10^{-4}, 10^{-3}, 5 \times 10^{-3}$ and 10^{-2}.

References

[1] T.J Poinsot and S.K Lele. Boundary conditions for direct simulations of compressible viscous flows. *J. Comput. Phys.*, 101(1):104–129, 1992.